

Geological Field Trips and Maps

2021
Vol. 13 (1.2)



ISSN: 2038-4947



Morphodynamic and sedimentary processes in salt-marshes and tidal channels of the Venice Lagoon (Italy)

**Tidalites 2022 - 10th Congress of Tidal Sedimentology.
Pre-congress Field Trip T4, Matera, Italy**

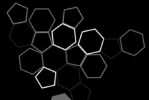
<https://doi.org/10.3301/GFT.2021.02>



*Società Geologica
Italiana*



ISPRA
Dipartimento per il
SERVIZIO GEOLOGICO D'ITALIA
Organo Cartografico dello Stato (legge n°68 del 2-2-1960)



Sistema Nazionale
per la Protezione
dell'Ambiente

GFT&M - *Geological Field Trips and Maps*

Periodico semestrale del Servizio Geologico d'Italia - ISPRA e della Società Geologica Italiana
Geol. F. Trips Maps, Vol. **13** No.1.2 (2021), 35 pp., 14 Figs. (<https://doi.org/10.3301/GFT.2021.02>)

Morphodynamic and sedimentary processes in salt-marshes and tidal channels of the Venice Lagoon (Italy)

Tidalites 2022 - 10th Congress of Tidal Sedimentology. Pre-congress Field Trip T4, Matera, Italy

Massimiliano Ghinassi¹, Andrea D'Alpaos¹, Alvise Finotello², Sonia Silvestri³, Elena Bellizia¹, Marta Cosma¹

¹ Department of Geosciences - University of Padova - Italy

² Department of Environmental Sciences, Informatics and Statistics, Ca' Foscari - University of Venice - Italy

³ Department of Biological, Geological, and Environmental Sciences - University of Bologna - Italy

Corresponding Author e-mail address: massimiliano.ghinassi@unipd.it

Responsible Director

Claudio Campobasso (ISPRA-Roma)

Editor in Chief

Andrea Zanchi (Università di Milano-Bicocca)

Editorial Manager

Angelo Cipriani (ISPRA-Roma)

Silvana Falcetti (ISPRA-Roma)

Fabio Massimo Petti (Società Geologica Italiana - Roma)

Diego Pieruccioni (ISPRA - Roma)

Alessandro Zuccari (Società Geologica Italiana - Roma)

Associate Editors

M. Berti (Università di Bologna), *M. Della Seta* (Sapienza Università di Roma),

P. Gianolla (Università di Ferrara), *G. Giordano* (Università Roma Tre),

M. Massironi (Università di Padova), *M.L. Pampaloni* (ISPRA-Roma),

M. Pantaloni (ISPRA-Roma), *M. Scambelluri* (Università di Genova),

S. Tavani (Università di Napoli Federico II)

Technical Advisory Board for Geological Maps

F. Capotorti (ISPRA-Roma), *F. Papasodaro* (ISPRA-Roma),

D. Tacchia (ISPRA-Roma), *S. Grossi* (ISPRA-Roma),

M. Zucali (University of Milano), *S. Zanchetta* (University of Milano-Bicocca),

M. Tropeano (University of Bari), *R. Bonomo* (ISPRA-Roma)

Editorial Advisory Board

D. Bernoulli, *F. Calamita*, *W. Cavazza*, *F.L. Chiocci*, *R. Compagnoni*,

D. Cosentino, *S. Critelli*, *G.V. Dal Piaz*, *P. Di Stefano*, *C. Doglioni*,

E. Erba, *R. Fantoni*, *M. Marino*, *M. Mellini*, *S. Milli*,

E. Chiarini, *V. Pascucci*, *L. Passeri*, *A. Peccerillo*, *L. Pomar*,

P. Ronchi, *B.C. Schreiber*, *L. Simone*, *I. Spalla*, *L.H. Tanner*,

C. Venturini, *G. Zuffa*.

Cover page Figure: Meandering tidal channels cutting through salt marshes of the Northern Venice Lagoon

ISSN: 2038-4947 [online]

<http://gftm.socgeol.it/>

The Geological Survey of Italy, the Società Geologica Italiana and the Editorial group are not responsible for the ideas, opinions and contents of the guides published; the Authors of each paper are responsible for the ideas, opinions and contents published.

Il Servizio Geologico d'Italia, la Società Geologica Italiana e il Gruppo editoriale non sono responsabili delle opinioni espresse e delle affermazioni pubblicate nella guida; l'Autore/i è/sono il/i solo/i responsabile/i.

INDEX

Information

Abstract 4
 Program summary 4
 Safety 5
 Hospitals 5
 Accommodation 5

Excursion notes

1. Introduction and aim of the field trip 7
 2. Regional geological and geomorphological setting..... 7

Itinerary

DAY 1: Bio-geomorphological features of salt-marshes, tidal flats and tidal channels cutting through them... 12
Stop 1.1: Salt-marshes and halophytic vegetation (45°29'43.58"N; 12°28'22.70"E) 13
Stop 1.2: Lateral shifts of salt-marshes edges (45°30'27.46"N; 12°28'16.12"E) 14

Stop 1.3: Initiation of tidal channels (45°28'34.73"N; 12°27'48.75"E) 16

DAY 2: Small-scale tidal meandering channels and related deposits. 18

Stop 2.1: Evolution of tidal networks (45°28'36.25"N; 12°27'28.22"E) 19

Stop 2.2: An abandoned meander and its deposits (45°28'38.66"N; 12°27'30.13"E) 20

Stop 2.3: A translating meander bend and its deposits (45°28'40.20"N; 12°27'28.41"E) 22

Stop 2.4: Cuspate meanders and their planform evolution (45°28'39.76"N; 12°27'25.20"E) 24

DAY 3: Morphodynamics and sedimentology of a large-scale meander bend..... 27

Stop 3.1: Interaction between lateral tributaries and the main channel (45°28'53.10"N; 12°26'59.31"E)..... 28

Stop 3.2: Morphodynamics and sedimentology of a large-scale tidal channel (45°28'41.56"N; 12°26'57.69"E)..... 29

References 32

Abstract

Tidal landscapes are currently threatened by climate change and increasing human interferences, and are possibly subject to irreversible transformations with far-reaching social, economical, and ecological implications worldwide. The Venice Lagoon formed over the last 7500 years and represents an outstanding example of tidal landscapes where natural and anthropic processes coexist. The Venice Lagoon is a peerless laboratory to study the deposits associated with salt-marshes, tidal flats, and tidal channels under variable rates of subsidence and sediment supply. Investigations on salt marshes and tidal channels of the Venice Lagoon can provide precious insights to understand morphodynamic processes typifying microtidal lagoonal environments worldwide.

Key words

salt-marshes, halophytic vegetation, tidal meanders, tidal point-bars, morphodynamic evolution.

Program summary

During this field trip, we will observe salt-marshes, tidal flats, and tidal channels of the northern lagoon, which is the most naturally preserved area of the entire lagoon. Salt-marshes and tidal flats will be visited to observe surface morphologies, the distribution of halophytic vegetation, and variability of sedimentary features, whereas active and abandoned meandering tidal channels will be observed with the main goal to link their morphodynamic evolution to the related sedimentary features.

Day1: Bio-geomorphological features of salt-marshes, tidal flats, and tidal channels cutting through them.

This first itinerary (Fig. 1) focuses on the main features of salt-marsh systems by analyzing the interactions between physical and biological processes that are responsible for the development of peculiar bio-geomorphic patterns (Saline and San Felice salt-marshes). Furthermore, this itinerary will also allow observation of a small meandering channel which displays spatially-varying erosional and depositional trends.

Day2: Small-scale tidal meandering channels and related deposits.

This second itinerary (Fig. 1) focuses on active and abandoned tidal meandering channels, whose widths range between 6 and 20 m. These meanders are also characterized by different modes of planform evolution and flow configurations, which will be discussed showing previously-acquired flow-velocity data.

Day3: Morphodynamics and sedimentology of a large-scale meander bend.

This third itinerary (Fig. 1) focuses on the sedimentology and morphodynamics of a meander bend formed by the Gaggian channel, which is a 100 m wide tidal channel. The role of tidal asymmetry in shaping meander bends will be discussed at this site.

Safety

The field trip is planned to consist of short walks in muddy areas, where rubber boots are required. Autumn in Venice is commonly warm, although windy days or brief showers can occur. Sun cream and hat are recommended along with a rain jacket. Minor changes in the order of the stops could be made following requirements dictated by tide conditions.

Emergency numbers:

112: Numero di emergenza Unico Europeo (European Emergency Number)

118: Pronto Soccorso (First aid)

115: Vigili del Fuoco (Fire brigade)

113: Polizia (Police)

Hospitals

Ospedale civile Mestre (Via Don Federico Tosatto 147, 30174, Venezia (VE) - telephone: +39 041 9656280)

Accommodation

Azienda Agrituristica La Barena (Via Lio Maggiore, 21, 30016 Jesolo VE)



Fig. 1 – Field trip itinerary, showing the location of stops of day 1 (1.1–1.3), day 2 (2.1–2.4), and day 3 (3.1– 3.2).



1. Introduction and aim of the field trip

Estuaries and lagoons are vulnerable coastal environments, which evolve under the combined effect of hydrological, chemical, and biological processes. Nowadays, the morphodynamic evolution of such coastal environments is influenced by anthropogenic pressures and the rapid climate changes that make predictions of the imminent evolution of estuarine systems quite a tricky issue. Therefore, understanding estuarine morphodynamics and sedimentology of the related deposits has noticeable economic and social implications both in terms of landscape management and subsurface exploration.

The city of Venice and its lagoon are included in the UNESCO World Heritage List of sites of extraordinary universal value and they also represent a great example of the intertwined coexistence between natural environment and processes, and human activities. To the purposes of this field trip, the Venice Lagoon represents a unique laboratory to expand current knowledge about the accumulation of salt-marsh, tidal flat and tidal channel deposits under the variability of natural forcings such as subsidence and sediment supply. During this trip, the most naturally preserved areas of the northern lagoon will be visited. In these areas, relative sea-level rise is ca. 3-4 mm/yr (Day et al., 1998) and is mainly balanced by salt-marsh sedimentation. Salt-marshes, tidal flats, and tidal channels cutting through them will be observed and analyzed to understand processes behind the development of surface morphologies and the distribution of halophytic vegetation and sediment grain-size. Moreover, active and abandoned tidal channels will be observed to discuss their origin and morphodynamic evolution. During the trip, sediment dry-peels of cores recovered from these different depositional sub-environments will be shown and analyzed to examine their characteristics in terms of sedimentary processes and dynamics.

2. Regional geological and geomorphological setting

The Venice Lagoon represents the largest Mediterranean brackish water body (total surface area of almost 550 km²) and forms an elongated, NE-SW basin, which is 50 km long and 10 km wide. The lagoon is limited by the deltaic system of the Piave River to the northeast, and by the Brenta, Adige, and Po rivers to the south-west. The Venice Lagoon is located in the coastal sector of the Venetian Plain, which is the foreland basin that developed between the South-Alpine and Apennine chains since the late Oligocene (Massari et al., 2009). After experiencing deep-water deposition, during the Early Pleistocene, the basin was filled up with a 750 m-thick succession of shallowing-upward deposits, spanning from turbidites to shallow marine ones (Massari



et al., 2004). Starting from the Middle Pleistocene, glacio-eustatic fluctuations brought to the alternation of coastal and continental conditions (Kent et al., 2002). Then, during the Last Glacial Maximum (LGM), the Venice city area was part of the distal sector of the Brenta river megafan (Fontana et al., 2014), experiencing alluvial deposition. Successively, between the end of the LGM and the Early Holocene, the coastal systems started starving with sediments and paralic deposition started (Amorosi et al., 2008). After that, the Holocene transgression promoted the formation of the lagoon – estuarine – barrier systems in the northern epicontinental Adriatic shelf through the flooding of the LGM alluvial plain (Zecchin et al., 2009, 2014), leading to the formation of the Venice Lagoon (last 7500 years). The Holocene succession (Fig. 2C) consists of three main units (Zecchin et al., 2008, 2009); the first one (up to 9 m thick) includes channelized deposits (distributary and/or estuarine channel fills), the second one (up to 10 m thick) is made of shoreface–shelf deposits and ebb-tidal deltas that pass landward into back-barrier sediments, and the third unit is characterized by lagoon deposits that mostly accumulated under human influence.

Currently, the lagoon exchanges water, nutrients, and sediments with the Adriatic Sea through the three inlets of Lido, Malamocco, and Chioggia from North to South (Fig. 2A). At the inlets, water depth commonly exceeds 10 m, whereas the inner basin shows mean elevations of 1.5 m below the current mean sea level (msl). The lagoon is characterized by a semidiurnal micro-tidal regime, with a mean tidal range of 1.0 m and maximum astronomic oscillations of 0.75 m around msl, respectively (D'Alpaos et al., 2013). Within tidal channels, the maximum water velocity is generated by spring tides and is of the order of 0.5-1.0 m/s (Rinaldo et al., 1999). Astronomical tides are often overlapped by meteorological surges which can produce significantly high (low) tides when atmospheric pressure is low (high). The highest high tides can exceed 1.5 m above msl, and typically take place during fall and winter. In these seasons, high-tide surges are enhanced by strong sirocco winds blowing from SE, which cause episodic flooding of the city of Venice that are known as “*Acqua Alta*” events (Mel et al., 2014). In November 1966, the tide reached about 1.70 m above msl (1.94 above the Punta della Salute tidal gauge, for which the tide-level zero was approximately 24 cm lower than msl), marking the highest water level ever documented in the lagoon.

Over the last centuries, many man-made interventions have affected the Venice Lagoon morphodynamics. Firstly, by the end of the 18th century all the major rivers that used to debouch into the lagoon were deviated towards the open sea, to forestall the ongoing silting up of the lagoon. This immediately caused the absence of freshwater and fluvial sediment input within the lagoon (D'Alpaos, 2010). Secondly, massive jetties were built up at the inlets between 1882 and 1935 to allow bigger vessels to enter the lagoon (Carniello et al.,

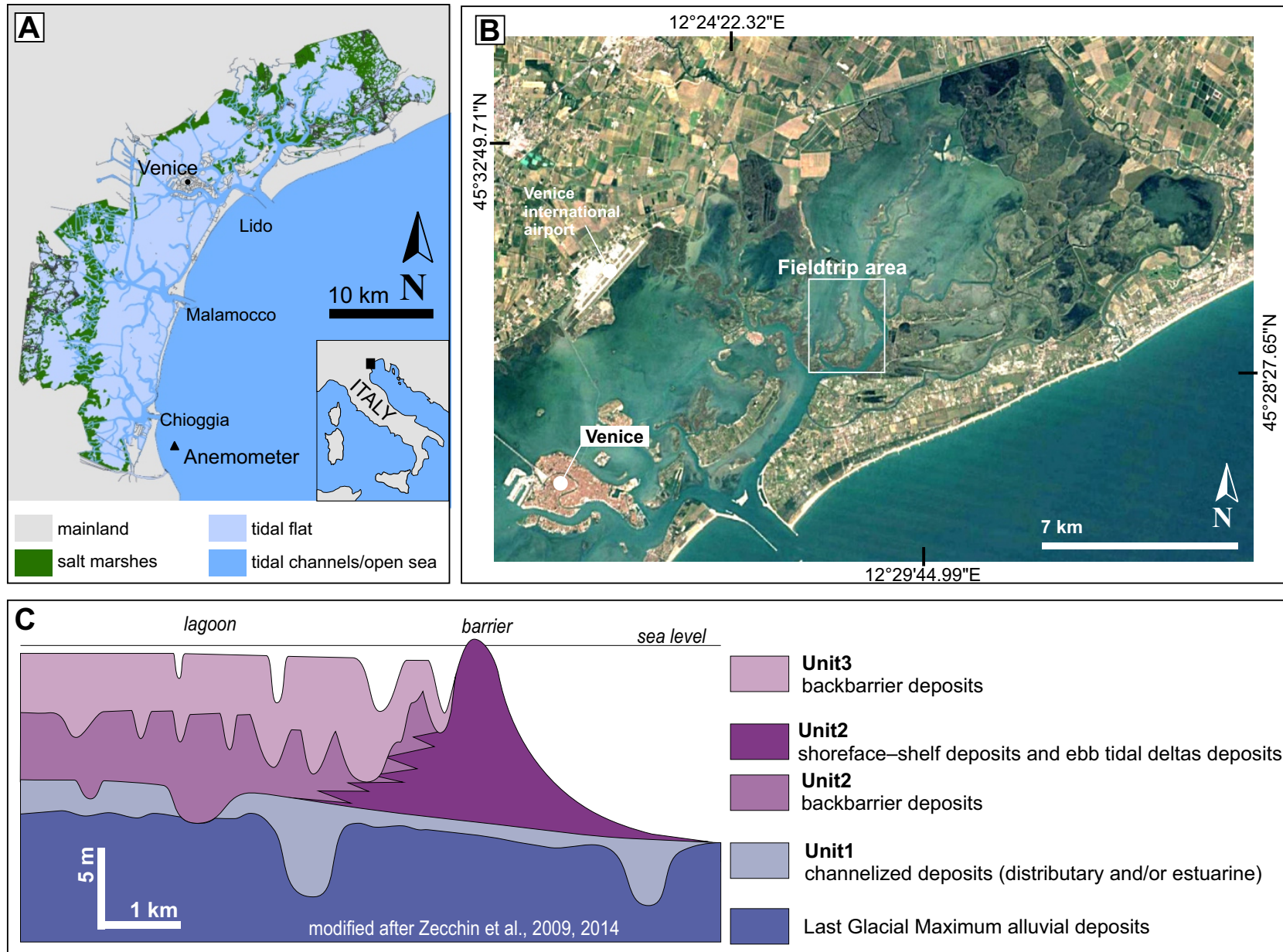


Fig. 2 - Field trip area. (A) Location of the Venice Lagoon along the northeastern coast of Italy. (B) Location of the field trip area in the northern Venice Lagoon. (C) Simplified architectural scheme of the Holocene deposits in the Venice Lagoon. Seismic units are shown (modified after Zecchin et al., 2009, 2014).



2009; D'Alpaos, 2010). This intervention caused relevant changes in the tidal regime within the lagoon, since currents became much more sustained than the typical periodic changes induced by the nodal modulation of the Adriatic Sea, which are in the order of 4% of the characteristic tidal range (Amos et al., 2010; Shaw and Tsimplis, 2010). Moreover, progressively greater portions of the lagoon became ebb-dominated, especially the areas surrounding the inlets where strong ebb-flood asymmetries increased the net export of sediments and prevented sediment supply from the open sea (Martini et al., 2004; Carniello et al., 2009; Ferrarin et al., 2015; Silvestri et al., 2018). This sediment loss caused the deepening of tidal flats and the overall decrease of salt-marsh areas (Carniello et al., 2009; D'Alpaos, 2010; Sarretta et al., 2010; Tommasini et al., 2019). Finally, considerable land reclamation for urban development and fish farming, carried out between 1930s and 1970s especially at the landward portions of the lagoon, caused a reduction of the total areas open to the diffusion of tides. During the same period, extraction of groundwater and natural gases for industrial purposes led to an increase in mean rate of relative sea level rise (typical value 3.5 mm/yr) by enhancing local subsidence rates up to 2 mm/yr (Gatto and Carbognin, 1981; Carbognin et al., 2004; Carniello et al., 2009; Ferrarin et al., 2015). Recently, a small reduction in the tidal amplitude and an increase in tidal phase delays within the lagoon, which consequently modified the internal hydrodynamic circulation, were caused by the installation of mobile gates at the inlets (Project Mo.S.E.), designed to protect Venice and other lagoon settlements from large floodings (Ghezzi et al., 2010; Matticchio et al., 2017).

Nowday salt-marshes and tidal flats within the lagoon are drained by a dense network of sinuous tidal channels, which commonly show a marked landward decrease in cross-sectional area (Marani et al., 2002; Lanzoni and D'Alpaos, 2015).

The study area of the San Felice salt-marshes (Fig. 2B) is located in the northern Venice Lagoon (i.e., the portion of the lagoon connected to the open sea through the Lido inlet), which is one of its most naturally preserved portions (Marani et al., 2003). The San Felice salt-marshes are characterized by an average elevation of about 0.30 m above msl and are colonized by a mosaic of halophytic species, among which *Spartina maritima*, *Limonium narbonense*, *Sarcocornia fruticosa* and *Juncus maritimum* (Silvestri et al., 2003, 2005; Belluco et al., 2006; Roner et al., 2016). The San Felice area was partly affected by the activity of the Piave River that used to flood the lagoon basin during the Late Holocene until the 17th century (Bondesan and Furlanetto, 2012).

The northern Venice Lagoon shows a mean temperature value of about 11°C and water salinity around 32 psu (Venier et al., 2014). The ongoing erosion of the marsh edges and the slow flooding of marsh surfaces are strongly influenced by waves generated by the Bora wind that blows from the NE during winters (up to 18



m/s during storm events) (Carniello et al., 2011). Wind-waves that impact against salt-marsh margins, have a wave period between 0.5 and 3.0 s and a wave height up to 0.6 m (Carniello et al., 2011; Marani et al., 2011; Tommasini et al., 2019). The average wind velocity is around 2.5 m/s, and measured turbidity values are about 22 FTU (suspended sediment concentration (SSC) around 20.7 mg/l, see Venier et al., 2014).



DAY 1:
Bio-geomorphological features of salt-marshes, tidal flats and tidal channels cutting through them.



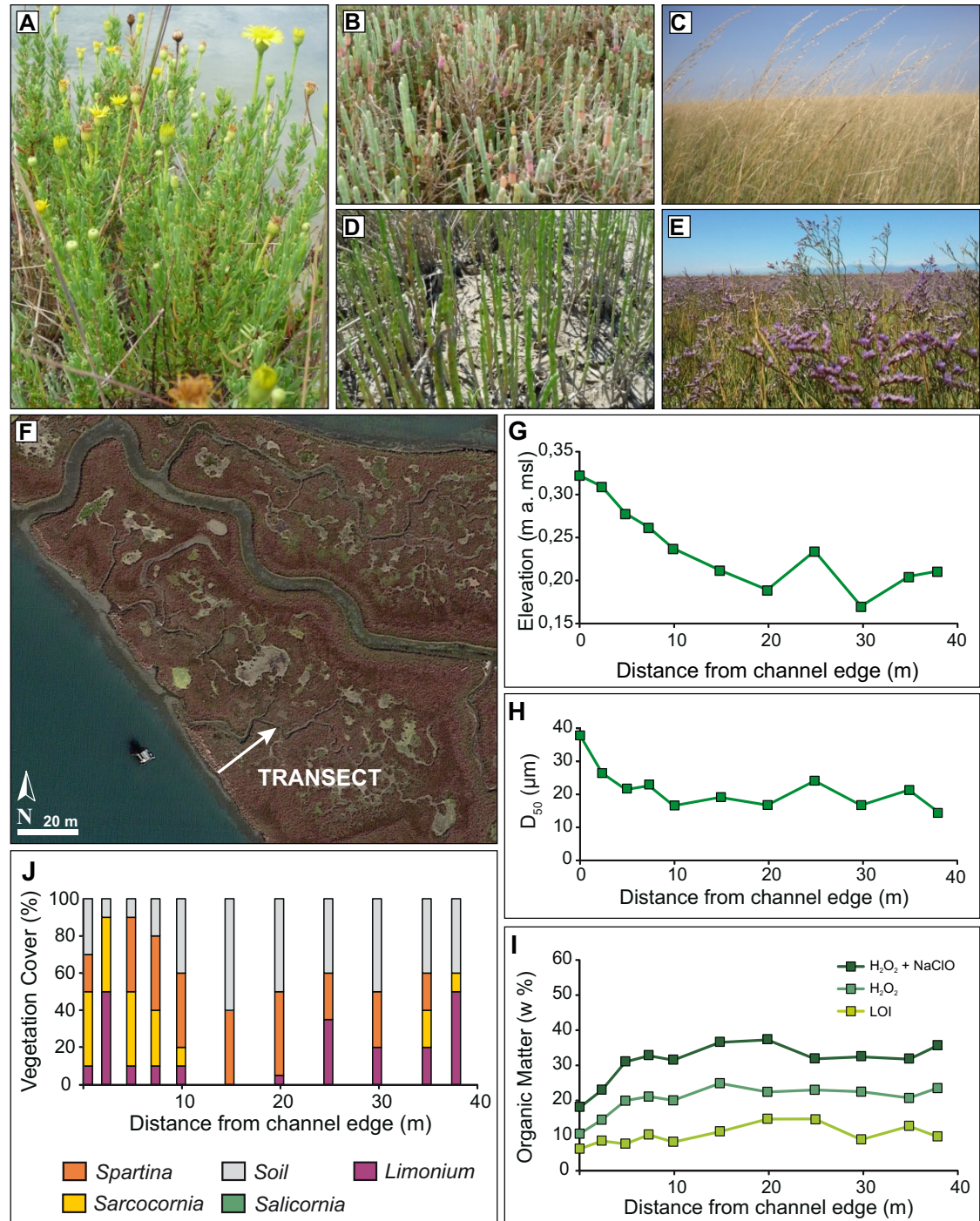
Fig. 3 - Location of stops 1.1–1.3 (day 1).



Stop 1.1: Salt-marshes and halophytic vegetation (45°29'43.58"N; 12°28'22.70"E)

Things to observe and discuss: the intertwined system composed by salt-marsh platforms and tidal channel networks cutting through them; the typical geomorphological and ecological patterns along a transect from the channel edge to the inner marsh; zonation patterns: a fascinating example of interaction between biotic and abiotic processes (reference papers: Marani et al., 2013; D'Alpaos and Marani, 2016; Roner et al., 2016). Stop 1.1 focuses on the observation of typical bio-geomorphic patterns that characterize the Saline salt marsh of the Venice Lagoon and other marshes worldwide. Different species of halophytic vegetation populate the microtidal marshes of the Venice Lagoon (Fig. 4), such as *Inula crithmoides* (Fig. 4A), *Sarcocornia fruticosa* (Fig. 4B), *Spartina maritima* (Fig. 4C), *Salicornia veneta* (Fig. 4D)

Fig. 4 - Examples of halophytic species (A-E) populating salt-marshes of the Venice Lagoon: (A) *Inula crithmoides*; (B) *Sarcocornia fruticosa*; (C) *Spartina maritima*; (D) *Salicornia veneta*; (E) *Limonium narbonense*. (F) Saline salt-marsh, in the area of stops 1.1–1.2; the white line indicates the transect that will be analysed during stop 1.1. Relevant biogeomorphic features along the transect: (G) elevation above mean sea level; (H) median sediment diameter; (I) organic matter content evaluated through three different methods; (J) vegetation cover (adapted from Roner et al., 2016).





Limonium narbonense (Fig. 4E). These marshes commonly exhibit a concave-up profile (Fig. 4F). Higher elevations are measured close to the channel edges (that represent the sediment source for the marsh) and lower elevations characterize the inner portions of the marsh (Fig. 4G). Inorganic sediments show a variable distribution of grain-sizes between medium sand and clay, and grains along the marsh edges (i.e., tidal channel levee) are coarser and become gradually finer toward the inner marsh (Fig. 4H). Analyses reveal also that whereas the inorganic accretion rate decreases with distance from the channel, the organic accretion rate increases towards the marsh interior (Fig. 4I). Bottom elevations are closely connected to vegetation cover (Fig. 4J); *Sarcocornia fruticosa*, *Puccinellia palustris* and *Inula crithmoides* commonly grow on higher soils, along the edges of creeks and channels, whereas *Spartina maritima* usually occupies the inner areas of the marsh that show lower elevations than the edges. *Limonium narbonense* is widely observed in the intermediate areas (Silvestri et al., 2005).

This stop allows to observe the peculiar spatial distribution of halophytic vegetation over the salt marsh, that is characterized by the existence of vegetation “patches”. This characteristic partition is known as zonation (Chapman, 1964; Silvestri et al., 2003), in the sense of a mosaic of wide vegetation patches of quite uniform composition, that exhibit sharp transitions where small topographic gradients occur. These bio-geomorphic patterns are the signatures of the coupled effects of geomorphological and biological dynamics, and are related to the ability of vegetation to act as a landscape engineer by tuning local marsh elevation within preferential ranges of optimal adaptation (Marani et al., 2013).

Stop 1.2: Lateral shifts of salt-marshes edges (45°30'27.46"N; 12°28'16.12"E)

Things to observe and discuss: prograding marshes; lateral erosion of the marsh edge (reference papers: Marani et al., 2011; Tommasini et al., 2019).

Today, the Venice Lagoon is suffering from a severe erosional trend that results from several natural and anthropogenic forcing, such as the rate of relative sea level rise (on average equal to 3.0 - 4.0 mm/yr); the erosion of salt-marsh edges and tidal-flat bottoms due to wind waves; the absence of sediment input because of the river diversions carried out between the 15th and the 17th centuries by the Most Serene Republic of Venice (the Renaissance Venetian State); and finally, the hydrodynamic asymmetry caused by the jetties at the inlets, which leads to the loss of fine sediments towards the Adriatic sea during the ebb phases of the tide.

Nevertheless, a few cases show salt marshes characterized by vertical and lateral accretion. Sediments, produced from the erosion of tidal flats facing the marshes, are delivered over the marsh platform and on the marsh



borders by waves and tides. Figure 5 shows a comparison between satellite images taken in 2003 (Fig. 5A) and 2019 (Fig. 5B) in which the progressive erosion of the tidal flat (located to the East of the salt-marshes),

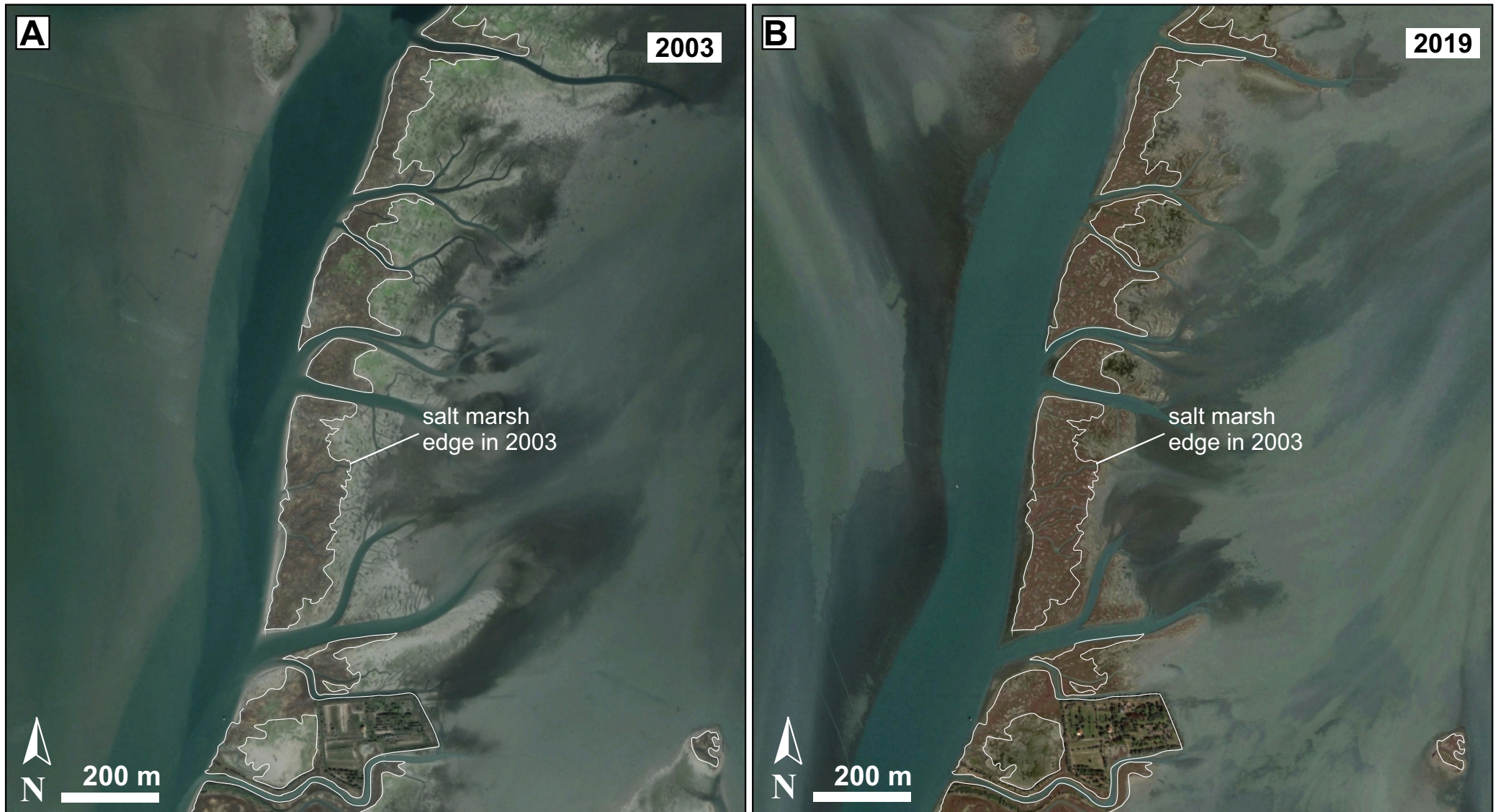


Fig. 5 - Google Earth images of the Saline salt-marsh in 2003 (A) and in 2019 (B). During stop 1.2 marsh vertical accretion, marsh progradation and the retreat of salt-marsh margins will be analyzed.



provides sediments for the vertical accretion and the horizontal progradation of the marshes. The dynamics of this coupled system composed by salt-marshes and the adjacent tidal flats will be analyzed also observing sedimentary cores collected in the field.

Stop 1.3: Initiation of tidal channels (45°28'34.73"N; 12°27'48.75"E)

Things to observe and discuss: the intertwined system composed by salt-marsh platforms and tidal channel networks cutting through them; the initiation of tidal channels: where do channels begin?; stratal architecture and migration of tidal meandering channels (reference papers: D'Alpaos et al., 2005; Stefanon et al., 2012).

Stop 1.3 focuses on the observation of the combined system represented by salt-marsh platforms and the channels they are dissected by. Tidal channels play an essential role in the evolution of salt-marsh systems since they represent preferential pathways for water, sediment, and nutrient transport. On the other hand, salt-marsh extent and elevation control the tidal prism that shapes channel cross sections: the larger the tidal prism, the larger the channel cross-sectional area, as dictated by the tidal prism – channel area relationship (see D'Alpaos et al., 2010 for channels within the Venice Lagoon). Furthermore, the tidal prism also controls the drainage density (the larger the tidal prism the larger the drainage density - Stefanon et al., 2012), which in turn provides a measure of the network efficiency in draining the tidal landscape.

The integration of different methodologies, such as morphometric and sedimentological analyses, and mathematical modeling, is crucial to improve the current knowledge about tidal meandering channels, by understanding their origin and evolution, and the sedimentary features emerging from their evolution. During this stop we will analyze a small meandering tidal channel (i.e., a creek) cutting through the San Felice salt-marsh. With a length of about 100 m, the creek ranges in width from 3.5 m to 0.7 m when moving towards the inner marsh, and its depth spans between 60 cm to just 5 cm. Mathematical models allowed the analysis of the planimetric configuration of the channel (determined through the use of high resolution (1 cm) images obtained through UAV) by quantitatively defining relevant geomorphic indicators, such as the morphological characteristics of the meandering channel (Marani et al., 2002), the drainage density (Marani et al., 2003), and the distribution of the bottom shear stresses (D'Alpaos et al., 2005). High-resolution sedimentological analyses, carried out on about 100 cores collected across 16 transects (Fig. 6A), revealed a general absence of filling deposits at the channel tips (from transect 1 to 4) thus showing an erosive trend (Fig. 6D). At transect 4, we observe deposition of mud, which suggests a shift from an erosive trend to a more depositional one (Fig. 6B). The sediment grain-size



increases from the channel head towards the outlet section, where sandy point-bar deposits occur (Fig. 6E). Furthermore, the distribution of the computed bottom shear stresses, which is responsible for the erosion processes, highlighted that the network developed via headward growth. Finally, repeated DGPS surveys in time (2002 and 2015) highlighted that the channel was characterized by non-negligible migration rates and adapted to changes in the landscape-forming discharges by increasing its cross-sectional area (Fig. 6B, C).

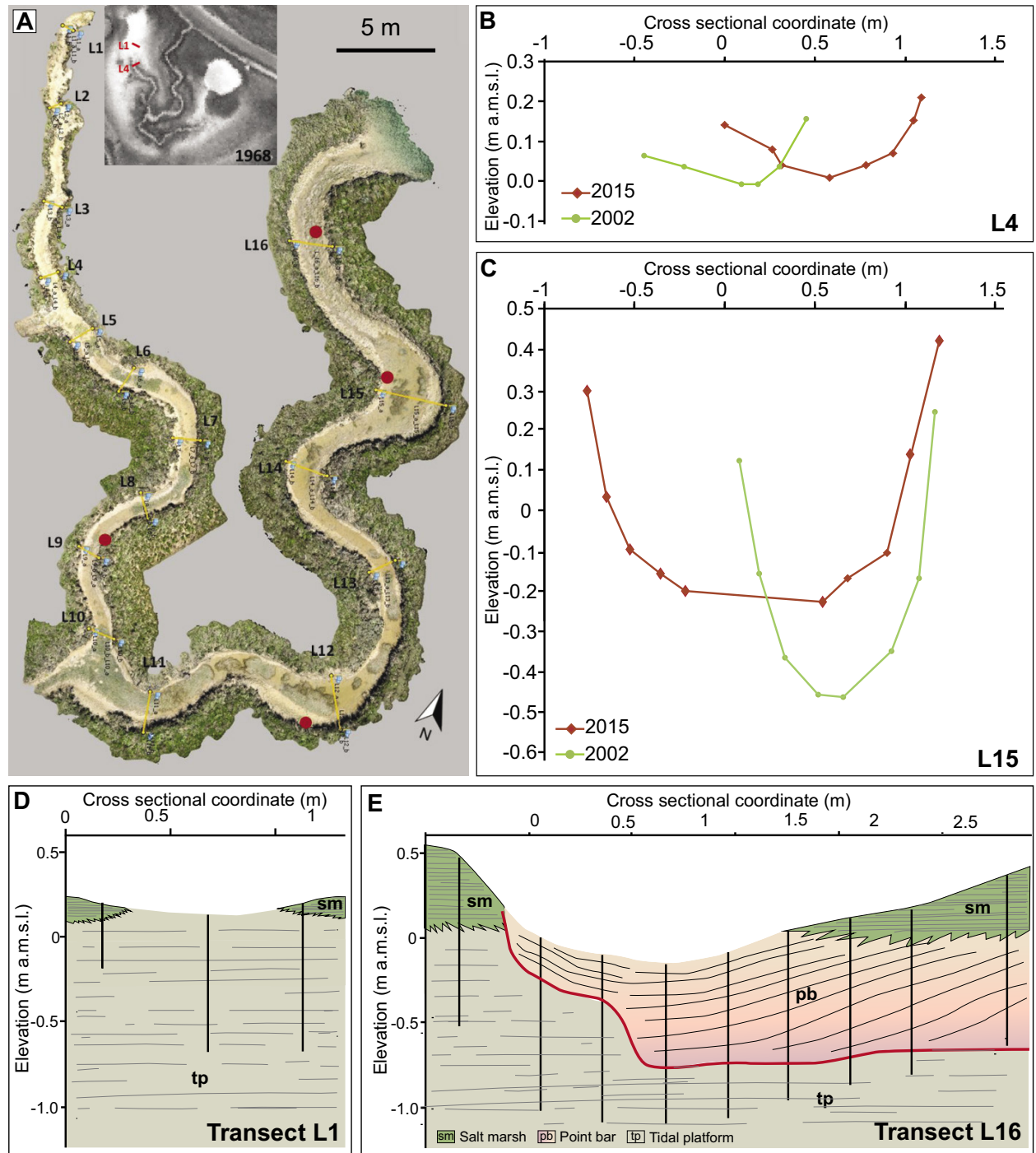


Fig. 6 - Small meandering tidal creek that will be analyzed during stop 1.3. (A) Planimetric configuration of the creek together with the location of sediment cores and of the cross sections surveyed with a DGPS. Comparison of channel cross sections in surveyed in 2002 and 2015 (B, C). (D, E) Stratigraphic architecture of two channel cross sections at the tips (D) and towards the seaward reach (E) of the meandering creek.

<https://doi.org/10.3301/GFT.2021.02>



DAY 2:

Small-scale tidal meandering channels and related deposits.



Fig. 7 - Location of stops 2.1-2.4 (day 2).



Stop 2.1: Evolution of tidal networks (45°28'36.25"N; 12°27'28.22"E)

Things to observe and discuss: active and abandoned tidal channels; rate of infill of abandoned channels; evolution of tidal networks following piracy events (reference paper: Cosma et al., 2020).

Stop 2.1 aims to focus the attention on both active and abandoned meandering tidal channels, which will be visited during this day. Some changes in the channel network, such as the abandonment of a meander bend and a piracy event, have been highlighted by the comparison between georeferenced 1938-1968 aerial photos. While the abandonment of the meander bend occurred during the 1950s and will be the goal of Stop 2.2, this first stop will be focused on the piracy event. Specifically, this peculiar event involved three main channels (labelled 1 to 3 in Fig. 8), and occurred when channel 1 pirated channel 3, causing the deactivation of the portion of channel 3 located seaward of the piracy site (branch named 3b in Fig. 8). This network reorganization favored sediment accumulation at the confluence between channels 2 and 3, and also caused the damming and



Fig. 8 - Comparison between the 1968 and present-day drainage evolution in the area of stops 2.1-2.4.



the following infill of channel 2. On the other hand, after the piracy event, channel 1 considerably increased its width seaward of the piracy site (branch named 1b in Fig. 8). After the piracy event, abandoned channels were almost entirely filled with mud. Nevertheless, branch 3b deposits were mainly eroded by the retreat of the San Felice channel bank (Fig. 8). The branches of channels 1 and 3 located upstream of the piracy site (named 1a and 3a in Fig. 8) are still active and host meander bends that will be observed at stops 2.3 and 2.4, respectively.

Stop 2.2: An abandoned meander and its deposits (45°28'38.66"N; 12°27'30.13"E)

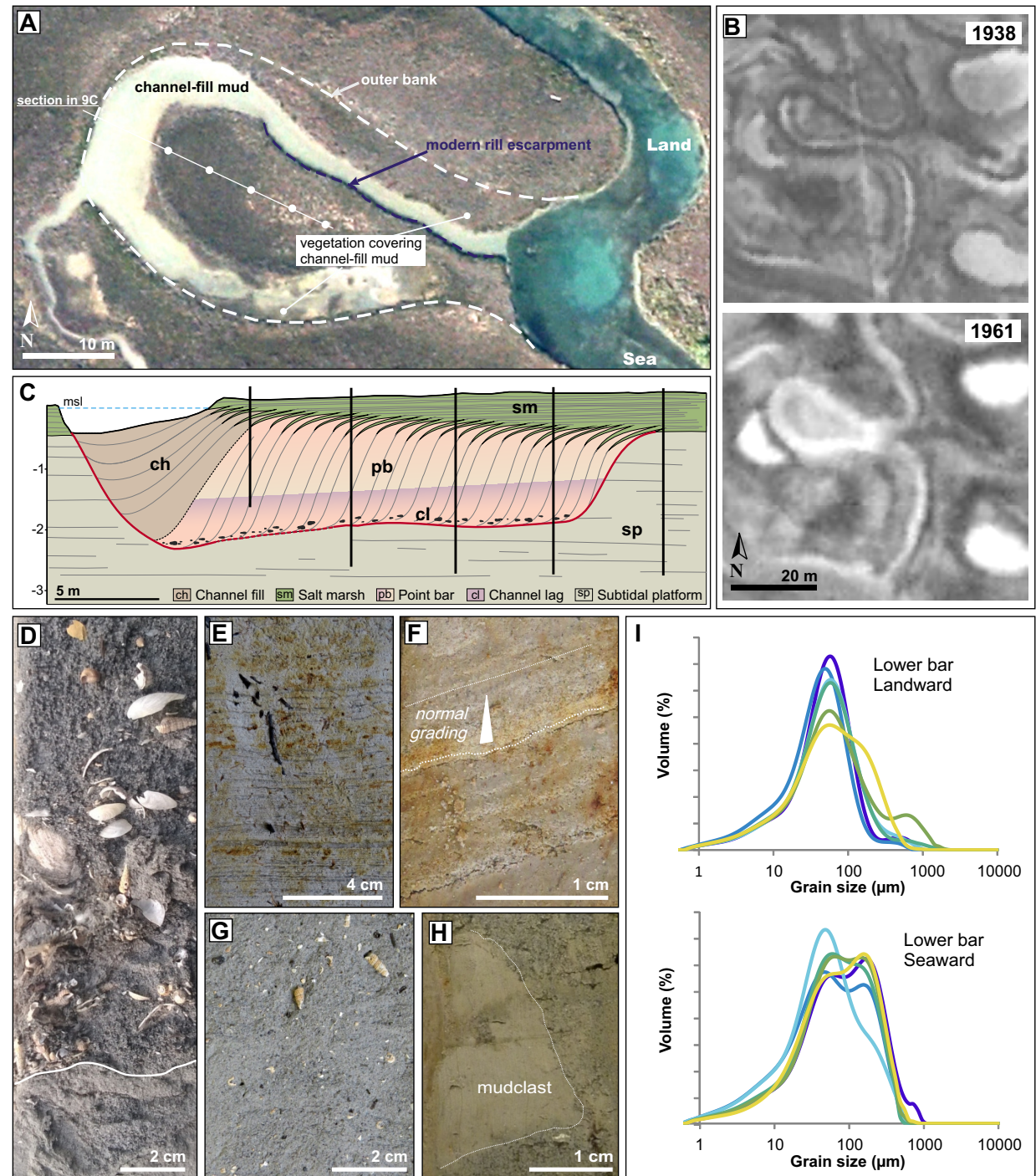
Things to observe and discuss: abandoned tidal meander, channel-fill deposits, infill rate of oxbow lakes, geometry of point-bar deposits, grain-size variability along tidal meander bends, relationship between vertical aggradation and lateral channel shift (reference papers: Brivio et al., 2016; D'Alpaos et al., 2017).

This stop focuses on an abandoned tidal meander loop that originated through a neck cut-off event of a bend defined by a 6-7 m-wide channel, which cuts through the salt-marsh. The loop is NW-SE oriented and is characterized by a simple symmetrical planform shape and a radius of curvature of about 13 m (Fig. 9A). The inner bank area (i.e., the point-bar top) shows a smooth topography, and there are no evident scroll-bar morphologies. The associated channel is almost completely filled with mud and is also locally colonized by halophytic vegetation. Nowadays, the landward reach of the loop is drained by a small rill that flows into the main active channel by cutting through the channel-fill and bar-top deposits (Fig. 9A). Moreover, although the extensive occurrence of halophytic vegetation, the outer bank of the channel is still visible. The analysis of the historical photos unveils that the meander cut-off event occurred during the 1950s (Fig. 9B) and was responsible for the progressive filling of the investigated channel with muddy deposits, which started accumulating on the seaward reach of the bend. The point-bar body associated with the abandoned bend overlies the heterolithic deposits of the subtidal platform with an erosive contact and is covered by both channel-fill and salt-marsh mud deposits. The bar is 1.5 - 1.7 m thick, and the maximum thickness of 1.9 m can be measured at the bend apex. Bar deposits are floored by a shell-rich lag characterized by massive medium sand with mud clasts (Fig. 9D, H). These deposits are overlaid by massive to stratified fine sand (Fig. 9G), that grades upward into laminated sandy mud (Fig. 9F). The upper portion of this sandy mud can be oxidized and is commonly composed of massive mud with millimeter laminae of well-sorted fine to very-fine sand, which sometimes exhibits some sharp erosional contacts and the normal grading (Fig. 9F). Salt-marsh deposits (Fig. 9E) are made of a horizontally-laminated oxidized mud, with a variable amount of fine to very-fine sand. This sand locally forms distinct laminae that resemble those occurring



in the uppermost portion of the bar. These deposits commonly show wood fragments, *in situ* roots and bioturbations (Fig. 9E). Overall, core data reveal that the sediment grain-size is almost uniform along the bar and both seaward and landward sides of the bend exhibit a comparable grain-size (Fig. 9I). Furthermore, the geometry of the point-bar base and bar top surface was defined through the spatial interpolation of core data (Fig. 9C). For instance, in a section parallel to the bend axis, the basal surface (i.e., channel-lag base) lowers down of about 0.8 m over a distance of 14 m; the point-bar top surface separates the point-bar body from the overlying salt marsh, and it shows a concave-upward, spoon-shaped geometry, whose axis runs parallel to that

Fig. 9 - Stop 2.2. (A) Aerial view of the abandoned meander bend; (B) comparison between the 1938 and 1961 configuration of the observed bend. (C) Cross section obtained correlating sedimentary cores recovered along the point-bar axis. (D) Shell-rich channel-lag deposits; (E) laminated salt-marsh mud; (F) millimetric sandy laminae within bar-top mud; (G) massive fine sand in the lower part of the bar; (H) mud clasts in the channel-lag deposits; (I) grain-size of lower bar deposits occurring in the seaward and landward side of the bar (6 samples for each site).





of the channel bend. This depression has a topographic relief of about 0.6 m, and its rim corresponds to the point-bar brink (i.e., inner bank of the abandoned channel).

Stop 2.3: A translating meander bend and its deposits (45°28'40.20"N; 12°27'28.41"E)

Things to observe and discuss: translating tidal meander, mutually-evasive currents, tidal asymmetry, point-bar vertical grain-size trend, migration rates of channels (reference papers: Ghinassi et al., 2018a; Finotello et al., 2020).

The tidal channel at stop 2.3 ranges in width between 15 and 20 m and cuts through a salt-marsh platform (Fig. 10A) overrun by different patches of halophytic vegetation. The meander bend has a "simple asymmetric" planform shape and its axis is trending ENE-WSW. It is also characterized by a radius of curvature of about 17 m and the channel depth varies from 3.0 to 2.0 m in the channel pool and riffle zones, respectively. The erosion affecting the landward side of the bar is responsible for the occurrence of bank collapses and a sub-vertical bank. These collapsed blocks are concentrated in the channel at the toe of the bank (Fig. 10E). The seaward side of the bar, which is depositional (Fig. 10D), is locally covered by sea grass and tilted between 10° and 15°. The deepest portion of the channel consists of medium-grained sand with abundant shells (Fig. 10C). Historical aerial photos show that, since the piracy event (see Stop 2.1), the accretion of the seaward side of the bar was in the order of 15 m (Fig. 10B), with an average migration rate of ~30 cm/yr. Accretion of these deposits gradually overlaid the confluence zone between channels 1 and 2. This bar shows a planform evolution corresponding to the process of translation (*sensu* Jackson, 1976).

At this site, flood and ebb phases of the tide exhibit different features in the flow velocity distribution. These measurements were carried out using an Acoustic Doppler Current Profiler (ADCP) at four different sections and results are shown in Fig. 10B (14th October 2014; tidal excursion ca. 40 cm). Data were collected at the maximum flood and ebb velocities, which come off when the water level is just above and below the elevation of the salt marsh, respectively.

Measurements reveal that during the flood phase flow velocities are high (ca. 35-40 cm/s) along the inner bank at section 1, whereas a minimum (ca. 5 cm/s) is measured along the outer bank. Moving landward, the maximum flow velocity tends to fall (ca. 25-35 cm/s) and moves toward the outer bank (sections 2 and 3), whereas quite a large eddy form close to the point-bar apex (section 3). At section 4 the flow velocity displays its maximum (ca. 35 cm/s) along the outer bank and the minimum (ca. 20 cm/s) along the inner bank. During



the ebb phase, the flow is almost uniform across section 4, where the high velocities (ca. 35-40 cm/s) are widely distributed. Moving seaward, the high velocity (ca. 35 cm/s) shifts toward the bar apex in section 3 and toward the outer (southern) bank in section 1, where a minimum of ca. 10 cm/s is measured along the inner bank. These measurements highlight that the seaward side of the bar is affected by strong and weak currents during flood and ebb tide stages, respectively (Fig. 10B).

Core data allowed to define the infill of a channel that was abandoned after the piracy event (channel 2 in Fig. 8), and the vertical grain-size distribution of bar deposits accreted along its seaward side since 1968. Point-bar

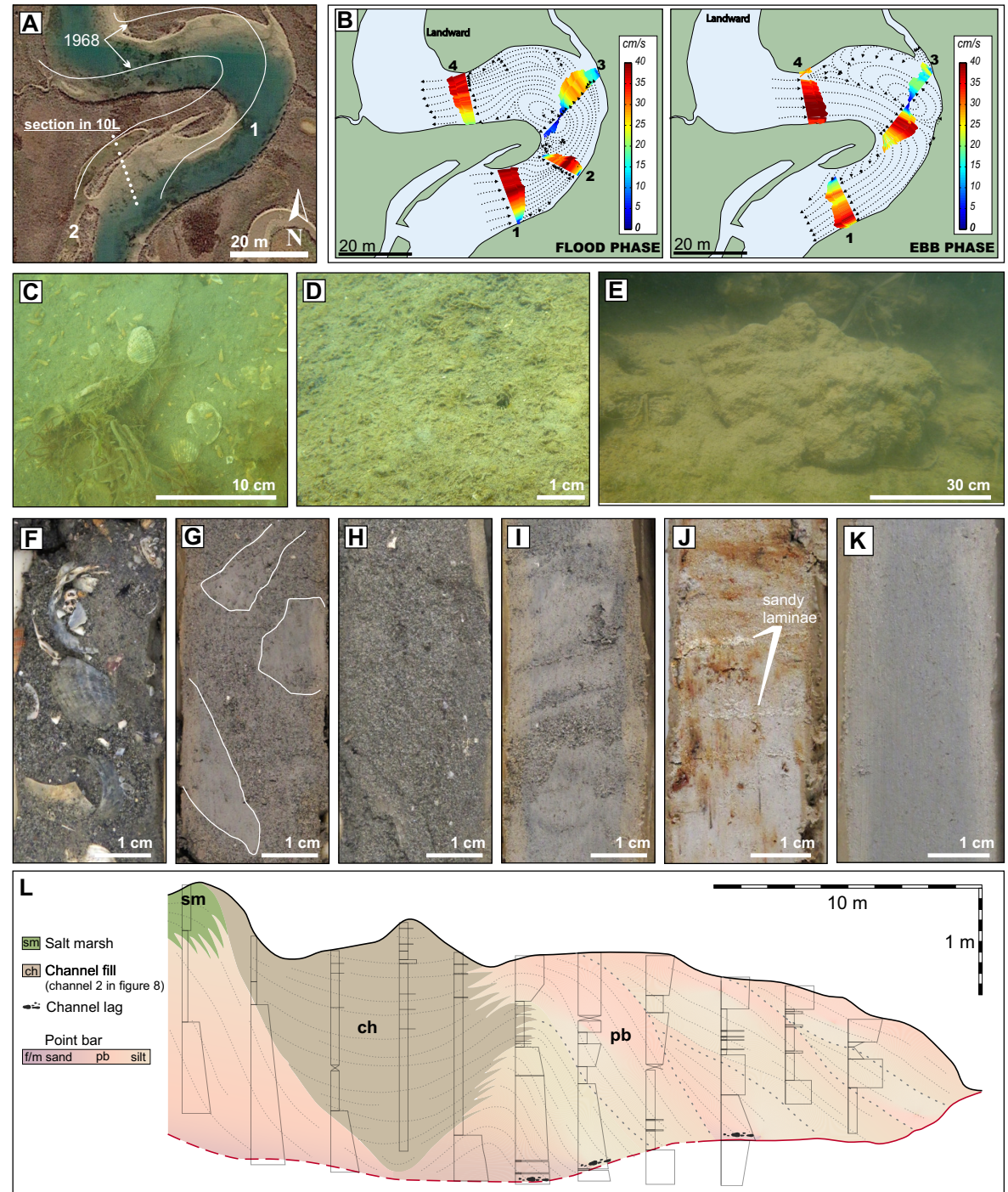


Fig. 10 - Stop 2.3. (A) Aerial view of the translating bar. Location of outer and inner bank in 1968 is shown; (B) flow-velocity configuration in ebb and flood conditions (October 2014); (C) thalweg of the present-day channel; (D) depositional surface along the seaward side of the bar; (E) collapsed block at the toe of the escarpment developed along the landward side of the bar; (F) shell-rich channel-lag sand; (G-H) sandy point-bar deposits; (I) heterolithic bar deposits; (J) bar top muddy deposits with millimetric sandy laminae; (K) massive channel-fill mud of channel 2 (see figure 6); (L) cross section obtained correlating sedimentary cores recovered in deposits accreted since the early 1970s.



deposits are up to 2.5 m thick and the channel lag is made of medium sand with abundant shells and mud clasts (Fig. 10F). Bar deposits are made of sand or sandy silt (Fig. 10H, I), and generally, sandy deposits contain a small amount of mud, that can form 1-3 mm-thick laminae. Sandy deposits appear mainly massive or weakly laminated, although severe bioturbation might impede the detection of specific small sedimentary structures. Overall, shells and shell fragments are not common, even if they can locally form 1-3 cm-thick layers. Where sandy deposits occur close to the boundary with the channel-lag sand, they commonly host dispersed pebble-sized mudclasts (Fig. 10G). Sandy silt deposits are made of greyish structureless silt with a variable amount of very fine to fine sand (Fig. 10I) and they show an inclined heterolithic stratification characterized by 1-5 mm-thick laminae with an inclination ranging between 5° and 15° (Fig. 10I) toward the channel. Within the sand of sandy silt deposits the muddy laminae do not show a clear rhythmic organization. In the uppermost part of the bar, where the muddy fraction is dominant, the inclined laminae consist of mud-free, well-sorted fine to very-fine sand (Fig. 10J). Medium sandy and sandy-silt deposits are organized into packages characterized by different vertical grain-size trends, such as fining-upward and fining- to coarsening-upward (Fig. 10L). This grain-size distribution leads to the occurrence of sandy deposits also in the middle-upper part of the bar. Channel-fill deposits of channel 2 are up to 2.2 m thick and consist of dark, structureless mud (Fig. 10K) with scattered bivalves in life position. Close to the top of these deposits, channel-fill ones can be either sandier or characterized by mottling and occurrence of root traces.

Stop 2.4: Cuspate meanders and their planform evolution (45°28'39.76"N; 12°27'25.20"E)

Things to observe and discuss: cuspate meander bends, outer-bank accretions, change of channel sinuosity, tidal sedimentary structures (reference paper: Finotello et al., 2020).

This stop focuses on the observation of tidal meanders generated by a 20 m-wide and 3 m-deep channel that shows cuspate planform geometries (Fig. 11B).

Acoustic Doppler Current Profiler (ADCP) was used to carry out flow velocity distribution measurements (19th July 2016; tidal excursion ca. 50 cm) at six different sections (Fig. 11E). As in stop 2.3, to detect the maximum ebb and flood velocities, data were collected when the water level was just below and above the elevation of the salt marsh, respectively. Maximum flow velocities (ca. 25 cm/sec) are systematically shifted along opposite sides of the channel by the tidal current turnover, with wide recirculating eddies developing on the sides located opposite to the maximum velocities. The inner bank of the bends is impinged by maximum



velocities during both flood and ebb phases along the seaward and landward sides of the bank, respectively.

By comparing present-day and 1938 configurations (Fig. 11A, B), the sinuosity of these bends appears to have decreased over the past 80 years. Specifically, sinuosity decreased from 1.34 to 1.21, and this mechanism occurred in parallel with a considerable channel widening from 11 to 17 m. This decrease in sinuosity is closely related to the accretion along the outer

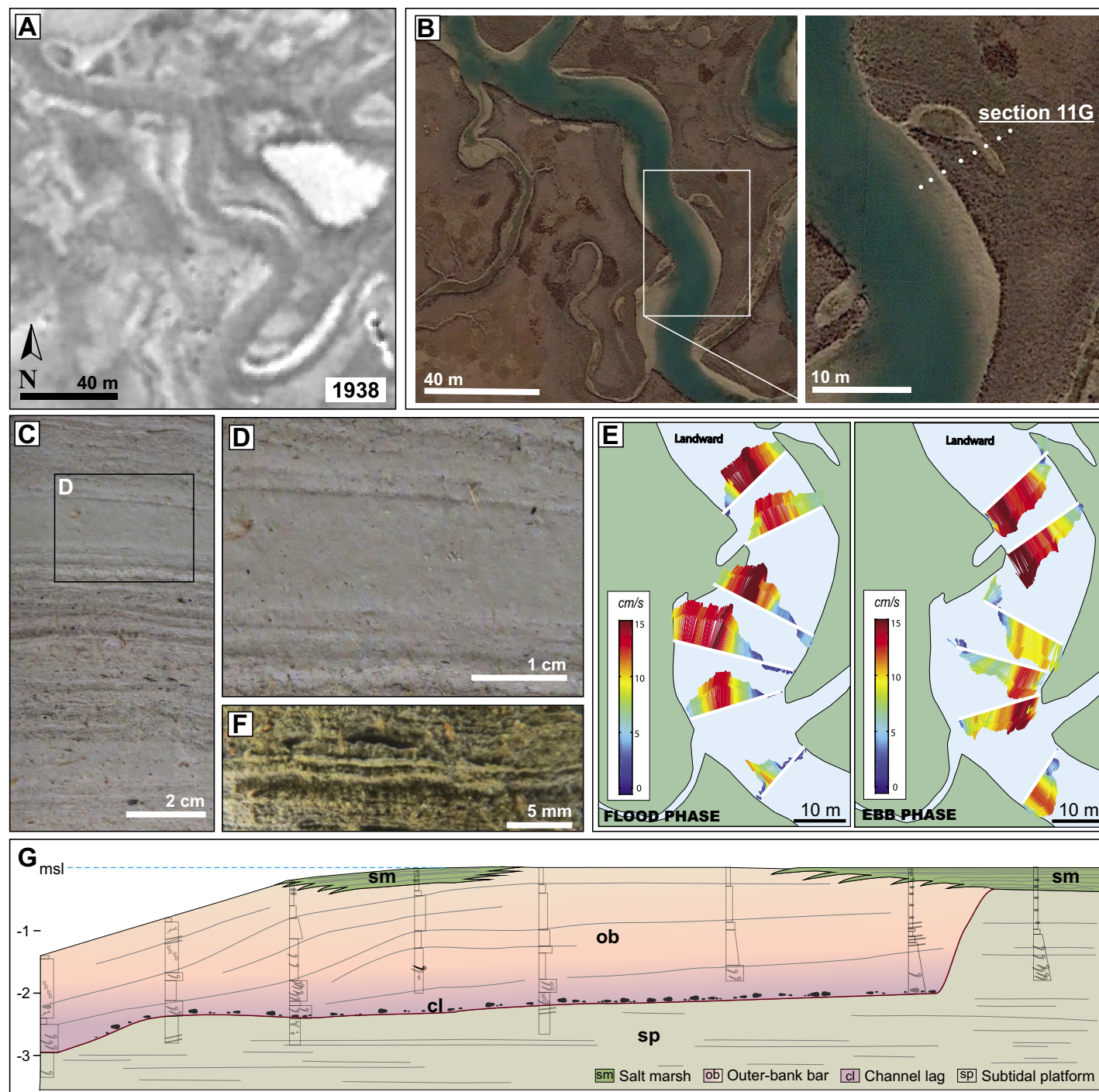


Fig. 11 - Stop 2.4. (A) Aerial view of the channel in 1938; (B) present-day configuration of the channel and location of cores used to define cross-section shown in G; (C) laminated mud in the upper part of the outer-bank deposits; (D) an anomalously thick layer made of massive mud; (E) ADCP data showing flow velocity distribution during ebbs and flood stages (F) double mud drapes; (G) cross section obtained correlating sedimentary cores recovered in the outer-bank deposits.



banks and the erosion of the point-bar apex, which occurred simultaneously with the shaping of a cusped bar planform.

Outer-bank deposits accreted toward the channel with a rate of about 0.15 cm/yr, and related deposits are 2.5-3 m thick. Sedimentary cores reveal that outer-bank is paved by a shell-rich, sandy basal lag (Fig. 11G) and then consists of medium-fine sand grading-upward into mud. Sandy deposits host a small amount of mud and are mainly structureless or weakly laminated. Furthermore, shells and shell fragments are common and are locally concentrated in 1-2 cm thick layers, and sand grades into mud with a transitional contact, where lamination is more pronounced. The overlying muddy interval is closely laminated (Fig. 11C), although laminae do not show any cyclic organization. Finally, double mud drapes separated by fine sand or silt can be observed (Fig. 11F), and there are isolated massive mud layers (up to 2 cm thick) (Fig. 11C, D).



DAY 3: Morphodynamics and sedimentology of a large-scale meander bend.



Fig. 12 - Location of stops 3.1 and 3.2 (day 3).



Stop 3.1: Interaction between lateral tributaries and the main channel (45°28'53.10"N; 12°26'59.31"E)

Things to observe and discuss: relationship between lateral tributaries and the main channel, development of a barb and related barb channel, vertical grain-size trend in barb deposits (reference papers: Ghinassi et al., 2018b; Finotello et al., 2019; 2020).

The main focus of this stop is the Gaggian Channel, which is a 100 m-wide and 7.5-8 m-deep channel that forms two adjacent bends, named hereafter Bend 1 and Bend 2 (Fig. 13A). Bend 1 develops around a point-bar with a mean radius of curvature of about 250 m (Fig. 13A) and shows tributaries on both the inner and the outer banks. Its two main tributaries are located along the outer bank of the bend and are named here as TW (Western Tributary) and TE (Eastern Tributary), respectively. These tributaries connect the Gaggian channel with the La Centrega tidal flat by entering the channel near the bend apex (Fig. 13A). Bend 2 forms a point-bar with a mean radius of curvature of about 200 m, and is characterized by the occurrence of an elongated sediment accumulation (named as "barb"). The barb is ca. 180 m long and is welded to the point apex and gradually becomes detached moving seaward (Fig. 13A). The analysis of georeferenced 1938-2016 aerial photos (Fig. 13A, B) highlights that the Gaggian Channel progressively widened from 83 m to 110 m. Over these 78 years, Bend 1 sinuosity poorly changed from 1.54 to 1.61. The photographic comparison shows also that along the seaward and landward sides of the bend, the inner bank accreted of ca. 5 and 25 m, respectively. Simultaneously, Bend 2 appeared to be more stable and its sinuosity kept a constant value of about 1.05. Historical aerial photos further show that between 1938 and 1968 the TW and TE tributaries were narrower than today. Tributaries widening occurred in parallel with an upstream propagation of their drainage systems, which developed an efficient connection between the channels and the adjacent La Centrega tidal flat. The bottom of the modern channels consists of medium-grained sand and are representatives of the deepest part of the Gaggian channel, whereas fine-grained silty sand is found in shallower areas and along the thalweg of the TW and TE tributaries. Bathymetric data highlight that since 1932 the channel progressively deepened, by increasing its averaged depth from 4 to 5 m; the deepest portions of the channel decreased and expanded their depth from 6.5 m in 1932 to 8.15 m in 1970 (Fig. 13C). Furthermore, detailed bathymetric data from 1932 (Fig. 13C) confirm the lack of the barb along the seaward side of Bend 2 at the beginning of the past century. As a matter of fact, the barb was completely developed in 1970 (Fig. 13C). Barb deposits are found along the seaward side of Bend 2 (Fig. 13D). This ridge is almost 180m long and up to 3 m thick. The barb was cored in the central part up to

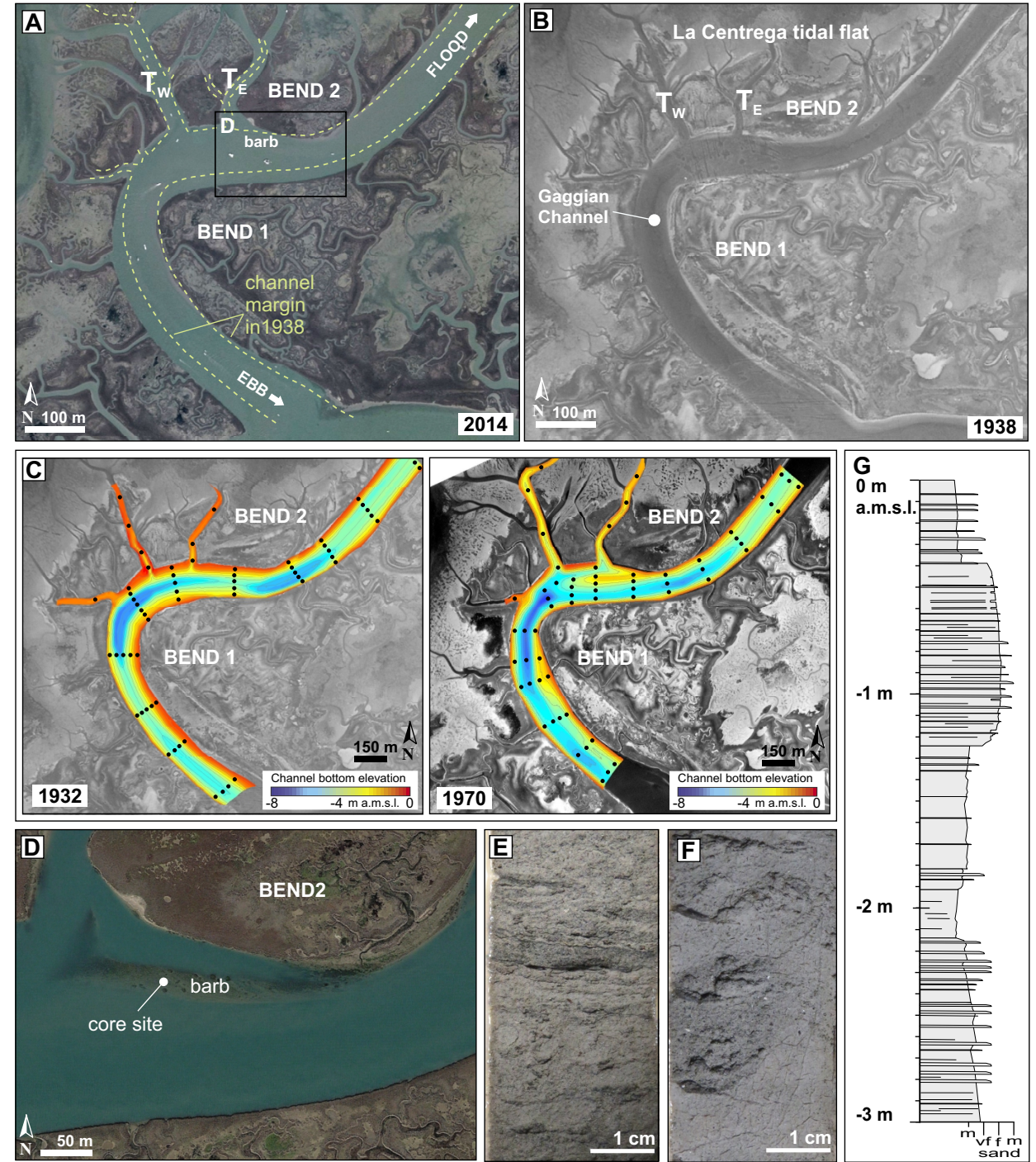


Fig. 13 - Stop 3.1. (A) Present-day configuration of the Gaggian Channel; (B) configuration of the Gaggian Channel in 1938; (C) bathymetric configuration of the channel in 1970 and 1932; (D) barb deposits accumulated along the seaward side of Bend 2; (E) laminated fine sand in the upper part of the barb body; (F) massive mud in the lower part of the barb body; (G) sedimentological log of the core recovered from the barb.

the depth of 3 m (Fig. 13G), and this core shows a vertical stacking of sand- and mud-prone deposits (Fig. 13E, F) that form 40-90 cm-thick intervals. Sandy deposits are made of plane-parallel laminated very-fine sand with silt and are rich in shells and shell debris, whereas laminations lack any clear cyclic organization. Muddy intervals are principally structureless, although they locally exhibit a poorly preserved plane-parallel lamination.

Stop 3.2: Morphodynamics and sedimentology of a large-scale tidal channel (45°28'41.56"N; 12°26'57.69"E)

Things to observe and discuss: accretion of tidal point-bars, vertical grain-size trend, absence of rhythmic deposition,



<https://doi.org/10.3301/GFT.2021.02>



tidal asymmetry (Reference papers: Ghinassi et al., 2018b; Finotello et al., 2019; 2020).

This stop also focuses on the Gaggian channel by analyzing two of its bends, which are named here Bend 1 and 2. Bend 1 is up to 8.10 m deep, and hosts medium sand in its deepest portion. Nevertheless, bedforms were observed neither in the thalweg zone nor along the point-bar slope (Fig. 14B, C). Point-bar deposits of Bend 1 were investigated using sub-bottom profiles, and two main sections (G5 and G10 in Fig. 14A) are selected here to describe bar architecture. Sub-bottom profiles were compared with bathymetric configuration defined in 1932 (Fig. 14A), highlighting that bar deposits of the landward reach of Bend 1 (Fig. 14D) are truncated by the modern channel. This comparison reveals also that the present thalweg is located 2 m deeper and 35 m toward the south (i.e., toward the inner bank of Bend 1) than the 1932's configuration. On the other hand, along its seaward side, the bend

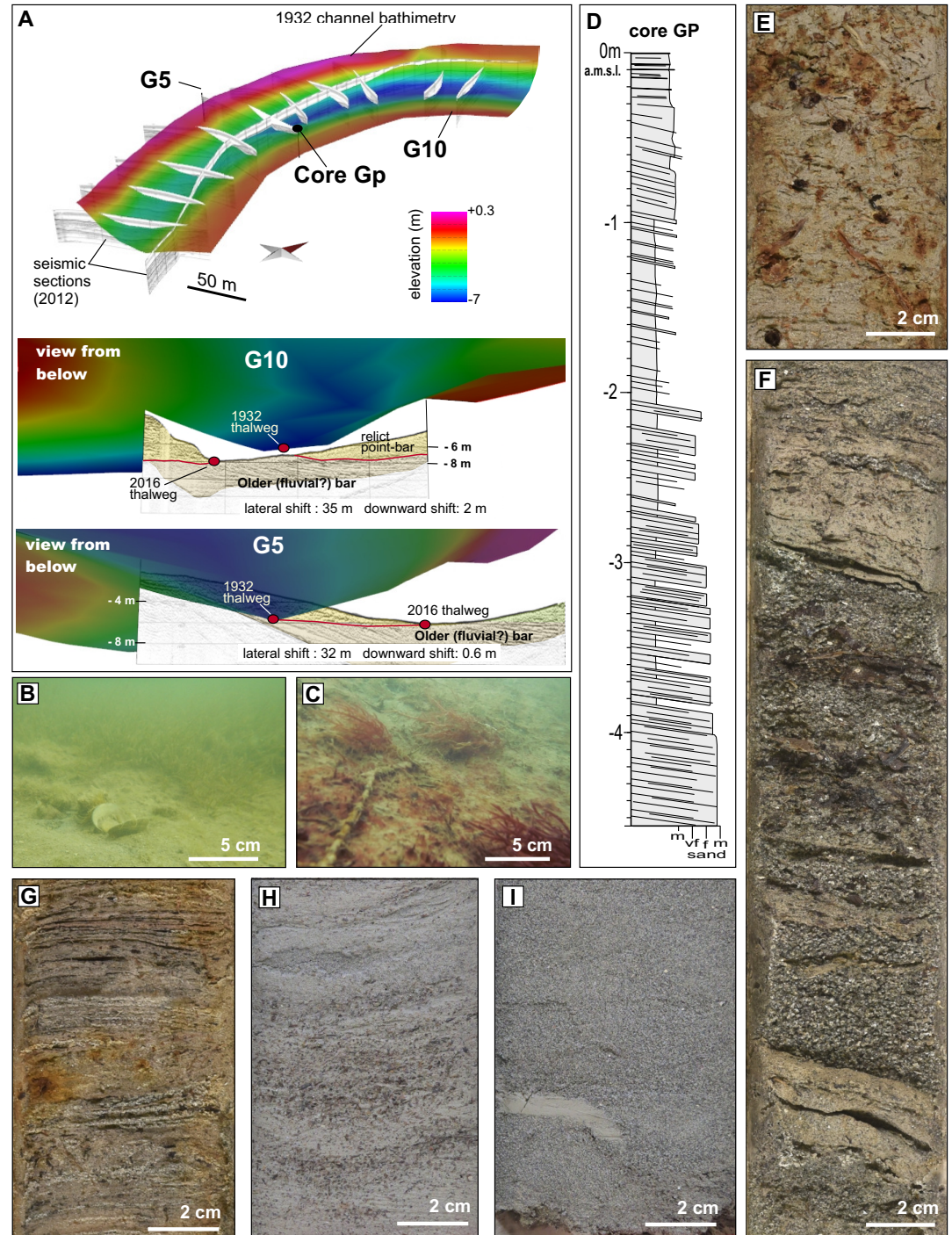


Fig. 14 - Stop 3.2. (A) Comparison between 1932 bathymetric configuration and sub-bottom profiles acquired in 2014; (B-C) digital images of the channel floor at -1 (B) and -7 m (C) below sea level; (D) sedimentological log of the core recovered along the seaward side of the bend; (E) salt-marsh mud on top of the core; (F) heterolithic deposits in the middle-lower part of the bar; (G-H) laminated mud underlying salt-marsh deposits with variable amount of plat debris; (I) massive sand with a pebble-sized mud clast in the lower part of the bar.



has accreted vertically of about 32 m and the thalweg moved downward almost 0.6 m. At core site Gp, deposits accreted along the seaward side of the Bend 1 were recovered (Fig. 14A) up to ca. 4.5 m from the bar top. Bar deposits are poorly stratified and contain sporadic mudclasts in the lower part (Fig. 14I), whereas they grade upward into an heterolithic interval consisting of laminated fine sand with 1-2 cm-thick mud layers (Fig. 14F). To the top, upper bar deposits are mainly muddy and poorly laminated, with a variable amount of plant debris (Fig. 14G, H), and finally, they are covered by massive and oxidized salt-marsh mud (Fig. 14E).

Acknowledgements

This work was supported by the University of Padova project "From channels to rock record: morphodynamic evolution of tidal meanders and related sedimentary products" (BIRD168939); and by the "HYDROSEM: Fluvial and tidal meanders of the venetian-Po plain: from hydrodynamics to stratigraphy" project (Progetto di Eccellenza CARIPARO 2017) which are gratefully acknowledged. S. Longhitano, A. Zanchi e F. Petti are kindly acknowledged for editorial assistance. The authors are indebted with J. Bartholdy and S. Mudd for reviewing the first version of this guide.

REFERENCES

- Amorosi A., Fontana A., Antonioli F., Primon S., Bondesan A. (2008) - Post-LGM sedimentation and Holocene shoreline evolution in the NW Adriatic coastal area. *GeoActa*, 7, 41-67.
- Amos C.L., Umgieser G., Tosi L., Townend I.H. (2010) - The coastal morphodynamics of Venice lagoon, Italy: An introduction. *Cont. Shelf Res.*, 30, 837-846.
- Belluco E., Camuffo M., Ferrari S., Modenese L., Silvestri S., Marani A., Marani M. (2006) - Mapping salt-marsh vegetation by multispectral and hyperspectral remote sensing. *Remote Sens. Environ.*, 105, 54-67.
- Bondesan A. and Furlanetto P. (2012) - Artificial fluvial diversions in the mainland of the Lagoon of Venice during the 16th and 17th centuries inferred by historical cartography analysis. *Géomorphol. Relief, Process, Environ.*, 18, 175-200.
- Brivio L., Ghinassi M., D'Alpaos A., Finotello A., Fontana A., Roner M., Howes N. (2016) - Aggradation and lateral migration shaping geometry of a tidal point-bar: An example from salt-marshes of the Northern Venice Lagoon (Italy). *Sediment. Geol.*, 343, 141-155.
- Carbognin L., Teatini P., Tosi L. (2004) - Eustacy and land subsidence in the Venice Lagoon at the beginning of the new millennium. *J. Mar. Syst.*, 51, 345-353.
- Carniello L., Defina A., D'Alpaos L. (2009) - Morphological evolution of the Venice Lagoon: Evidence from the past and trend for the future. *J. Geophys. Res.*, 114, 1-10.
- Carniello L., D'Alpaos A., Defina A. (2011) - Modeling wind waves and tidal flows in shallow micro-tidal basins. *Estuar. Coast. Shelf Sci.*, 92, 263-276.
- Chapman V.J. (1964) - *Coastal Vegetation*. Pergamon P. the Macmillan Company, New York.
- Cosma M., Finotello A., Ielpi A., Ventra D., Oms O., D'Alpaos A., Ghinassi M. (2020) - Piracy-controlled geometry of tide-dominated point-bars: Combined evidence from ancient sedimentary successions and modern channel networks. *Geomorphology*, 370, 107402.
- Day J.W., Rismondo A., Scarton F., Are D., Cecconi G. (1998) - Relative sea level rise and Venice lagoon wetlands. *J. Coast. Conserv.*, 4, 27-34.
- D'Alpaos L. (2010) - *Fatti e misfatti di idraulica lagunare. La laguna di Venezia dalla diversione dei fiumi alle nuove opere delle bocche di porto*. Istituto Veneto di Scienze, Lettere ed Arti: Venice.
- D'Alpaos A., Carniello L., Rinaldo A. (2013) - Statistical mechanics of wind wave-induced erosion in shallow tidal basins: Inferences from the Venice Lagoon. *Geophys. Res. Lett.*, 40, 3402-3407.
- D'Alpaos A., Ghinassi M., Finotello A., Brivio L., Bellucci L.G., Marani M. (2017) - Tidal meander migration and dynamics: A case study from the Venice Lagoon. *Mar. Pet. Geol.*, 87, 80-90.

- D'Alpaos A., Lanzoni S., Marani M., Fagherazzi S., Rinaldo A. (2005) - Tidal network ontogeny: Channel initiation and early development. *J. Geophys. Res.*, 110, 1-14.
- Ferrarin C., Tomasin A., Bajo M., Petruzzo A., Umgiesser G. (2015) - Tidal changes in a heavily modified coastal wetland. *Cont. Shelf Res.*, 101, 22-33.
- Finotello A., Canestrelli A., Carniello L., Ghinassi M., D'Alpaos A. (2019) - Tidal flow asymmetry and discharge of lateral tributaries drive the evolution of a microtidal meander in the Venice Lagoon (Italy). *J. Geophys. Res.*, 124(12), 3043-3066.
- Finotello A., Ghinassi M., Carniello L., Belluco E., Pivato M., Tommasini L., D'Alpaos A. (2020) - Three-dimensional flow structures and morphodynamic evolution of microtidal meandering channels. *Water Resour. Res.*, 56(7), e2020WR027822.
- Fontana A, Mozzi P, Marchetti M. (2014) - Alluvial fans and megafans along the southern side of the Alps. *Sediment. Geol.*, 301, 150-171.
- Gatto P. and Carbognin L. (1981) - The Lagoon of Venice: natural environmental trend and man-induced modification. *Hydrol. Sci. J.*, 26, 379-391.
- Ghezzi M., Guerzoni S., Cucco A., Umgiesser G. (2010) - Changes in Venice Lagoon dynamics due to construction of mobile barriers. *Coast. Eng.*, 57, 694-708.
- Ghinassi M., D'alpaos A., Gasparotto A., Carniello L., Brivio L., Finotello A., Roner M., Franceschinis E., Realdon N., Howes N., Cantelli A. (2018a) - Morphodynamic evolution and stratal architecture of translating tidal point-bars: Inferences from the northern Venice Lagoon (Italy). *Sedimentology*, 65, 1354-1377.
- Ghinassi M., Brivio L., D'Alpaos A., Finotello A., Carniello L., Marani M., Cantelli A. (2018b) - Morphodynamic evolution and sedimentology of a microtidal meander bend of the Venice Lagoon (Italy). *Mar. Pet. Geol.* 96, 391-404.
- Jackson R.G.I. (1976) - Depositional model of point-bars in the lower Wabash River. *J. Sediment. Petrol.*, 46, 579-594.
- Kent D.V., Rio D., Massari F., Kukla G., Lanci L. (2002) - Emergence of Venice during the Pleistocene. *Quat. Sci. Rev.*, 21, 1719-1727.
- Lanzoni S. and D'Alpaos A. (2015) - On funneling of tidal channels. *J. Geophys. Res.*, 120, 433-452.
- Marani M., Lanzoni S., Zandolin D., Seminara G., Rinaldo A., Zandolin D., Lanzoni S., Marani M., Rinaldo A. (2002) - Tidal meanders. *Water Resour. Res.*, 38, 7-14.
- Marani M., Belluco E., D'Alpaos A., Defina A., Lanzoni S., Rinaldo A. (2003) - On the drainage density of tidal networks. *Water Resour. Res.*, 39, 1-11.
- Marani M., D'Alpaos A., Lanzoni S., Santalucia M. (2011) - Understanding and predicting wave erosion of marsh edges. *Geophys. Res. Lett.*, 38, 1-5.
- Marani M., Da Lio C., D'Alpaos A. (2013) - Vegetation engineers marsh morphology through multiple competing stable states. *Proc. Natl. Acad. Sci. U.S.A.*, 110, 3259-3263.

- Martini P., Carniello L., Avanzi C. (2004) - Two dimensional modelling of flood flows and suspended sediment transport: the case of Brenta river, Veneto (Italy). *Nat. Hazards Earth Syst. Sci.*, 4, 165-181.
- Massari F., Grandesso P., Stefani C., Jobstraibizer P. (2009) - A small polyhistory foreland basin evolving in a context of oblique convergence: the Venetian basin (Chattian to Recent, Southern Alps, Italy). In: Allen P.A., Homewood P. (Eds.), *Foreland basins*. Blackwell Scientific: Oxford; 141-168.
- Massari F., Rio D., Serandrei Barbero R., Asioli A., Capraro L., Fornaciari E., Vergerio P.P. (2004) - The environment of Venice area in the past two million years. *Palaeogeogr. Palaeoclimatol. Palaeoecol.*, 202, 273-308.
- Matticchio B., Carniello L., Canesso D., Ziggliotto E., Cordella M. (2017) - Recent changes in tidal propagation in the Venice Lagoon: effects of changes in the inlet structure. *Venice. Atti Ist. Veneto Sci. Lett. Arti*, 60, 1-20.
- Mel R., Viero D.P., Carniello L., Defina A., D'Alpaos L. (2014) - Simplified methods for real-time prediction of storm surge uncertainty: The city of Venice case study. *Adv. Water Resour.*, 71, 177-185.
- Rinaldo A., Fagherazzi S., Lanzoni S., Marani M., Dietrich W.E. (1999) - Tidal networks 3. Landscape-forming discharges and studies in empirical geomorphic relationships. *Water Resour.*, 35, 3919-3929.
- Roner M., D'Alpaos A., Ghinassi M., Marani M., Silvestri S., Franceschinis E., Realdon N. (2016) - Spatial variation of salt-marsh organic and inorganic deposition and organic carbon accumulation: Inferences from the Venice lagoon, Italy. *Adv. Water Resour.*, 93, 276-287.
- Sarretta A., Pillon S., Molinaroli E., Guerzoni S., Fontolan G. (2010) - Sediment budget in the Lagoon of Venice, Italy. *Cont. Shelf Res.*, 30, 934-949.
- Shaw A.G.P. and Tsimplis M.N. (2010) - The 18.6 yr nodal modulation in the tides of Southern European coasts. *Cont. Shelf Res.*, 30, 138-151.
- Silvestri S., D'Alpaos A., Nordio G., Carniello L. (2018) - Anthropogenic modifications can significantly influence the local mean sea level and affect the survival of salt-marshes in shallow tidal systems. *J. Geophys. Res.*, 123, 996-1012.
- Silvestri S., Defina A., Marani M. (2005) - Tidal regime, salinity and salt-marsh plant zonation. *Estuar. Coast. Shelf Sci.*, 62, 119-130.
- Silvestri S., Marani M., Marani A. (2003) - Hyperspectral remote sensing of salt-marsh vegetation, morphology and soil topography. *Phys. Chem. Earth, Parts A/B/C* 28, 15-25.
- Stefanon L., Carniello L., D'Alpaos A., Rinaldo A. (2012) - Signatures of sea level changes on tidal geomorphology: Experiments on network incision and retreat. *Geophys. Res. Lett.*, 39, 1-6.
- Tommasini L., Carniello L., Ghinassi M., Roner M., D'Alpaos A. (2019) - Changes in the wind-wave field and related salt-marsh lateral erosion: inferences from the evolution of the Venice Lagoon in the last four centuries. *Earth Surf. Process. Landf.*, 44 (8), 1633-1646.
- Venier C., D'Alpaos A., Marani M. (2014) - Evaluation of sediment properties using wind and turbidity observations in the shallow tidal areas of the Venice Lagoon. *J. Geophys. Res.*, 119, 1604-1616.

- Zecchin M., Baradello L., Brancolini G., Donda F., Rizzetto F., Tosi L. (2008) - Sequence stratigraphy based on high-resolution seismic profiles in the late Pleistocene and Holocene deposits of the Venice area. *Mar. Geol.*, 253, 185–198.
- Zecchin M., Brancolini G., Tosi L., Rizzetto F., Caffau M., Baradello L. (2009) - Anatomy of the Holocene succession of the southern Venice lagoon revealed by very high-resolution seismic data. *Cont. Shelf Res.*, 29, 1343–1359.
- Zecchin M., Tosi L., Caffau M., Baradello L., Donnici S. (2014) - Sequence stratigraphic significance of tidal channel systems in a shallow lagoon (Venice, Italy). *The Holocene*, 24, 646–658.

*Manuscript received 12 October 2020; accepted 05 February 2021; published online 22 March 2021;
editorial responsibility and handling by S. Longhitano.*